Unexpectedly rapid aerosol formation in the Hunga Tonga plume

Elizabeth Asher, Michael Todt, Karen Rosenlof, Troy Thornberry, Ru-Shan Gao, Ghassan Taha, Paul Walter, Sergio Alvarez, James Flynn, Sean Davis, et al.

HAL Id: hal-04301363
https://hal.univ-reunion.fr/hal-04301363v1

Submitted on 24 Nov 2023

1   # Unexpectedly rapid aerosol formation in the Hunga Tonga plume

2

3   Elizabeth Asher[1,2a*], Michael Todt[1,2b], Karen Rosenlof[2], Troy Thornberry[2], RuShan Gao[2],
4   Ghassan Taha[3,4], Paul Walter[5], Sergio Alvarez[6], James Flynn[6], Sean Davis[2], Stephanie Evan[7],
5   Jerome Brioude[7], Jean-Marc Metzger[8], Dale F. Hurst[1,9], Emrys Hall[1,9], Kensy Xiong[1,9]

6

7   Elizabeth Asher easher@noaa.gov
8   Michael Todt michael.todt@colorado.edu
9   Karen Rosenlof karen.h.rosenlof@noaa.gov
10   Troy Thornberry troy.thornberry@noaa.gov
11   RuShan Gao rushan.gao@noaa.gov
12   Ghassan Taha ghassan.taha-1@nasa.gov
13   Paul Walter pauljw@stedwards.edu
14   Sergio Alvarez slalvare@central.uh.edu
15   James Flynn jhflynn@central.uh.edu
16   Sean Davis Sean.M.Davis@noaa.gov
17   Stephanie Evan stephanie.evan@univ-reunion.fr
18   Jerome Brioude jerome.brioude@univ-reunion.fr
19   Jean-Marc Metzger jean-marc.metzger@univ-reunion.fr
20   Dale F. Hurst dale.hurst@noaa.gov
21   Emrys Hall Emrys.Hall@noaa.gov
22   Kensy Xiong kensy.xiong@noaa.gov

23

24   [1] Cooperative Institute for Research in Environmental Sciences, University of Colorado Boulder,
25   216 UCB, Boulder, CO 80309, United States
26   [2] NOAA Chemical Sciences Laboratory, 325 Broadway, Boulder, CO 80305, United States
27   [3] Morgan State University, 1700 East Cold Spring Lane McMechen Hall Rm 635, Baltimore,
28   MD 21251, United States
29   [4] NASA Goddard Space Flight Center, 8800 Greenbelt Rd, Greenbelt, MD 20771, United States
30   [5] St. Edward's University, 3001 South congress, Austin, TX 78704, United States
31   [6] University of Houston, 4800 Calhoun Rd, Houston, TX 77004, United States
32   [7] Laboratoire de l'Atmosphère et des Cyclones (LACy), UMR8105, CNRS, Université de La
33   Réunion, Saint-Denis, France
34   [8] Observatoire des Sciences de l'Univers de la Réunion, UAR 3365 (CNRS, Université de la
35   Réunion, Météo-France), Saint-Denis, France
36   [9] NOAA Global Monitoring Laboratory, 325 Broadway, Boulder, CO 80305, United States
37   [a] Now at: NOAA Global Monitoring Laboratory
38   [b] Now at: Finnish Meteorological Institute (FMI), Helsinki, Finland
39   [*] Corresponding author

40

41   **Classification:** Physical Sciences, Atmospheric Sciences

42

43   **Keywords:** stratospheric aerosol, rapid aerosol formation, SO_2, volcanic plume, Hunga Tonga
44   eruption

45

46

Abstract

The Hunga Tonga-Hunga Haʹapai (HT-HH) volcanic eruptions on Jan. 13 and 15, 2022 produced a plume with the highest signal in stratospheric aerosol optical depth observed since the eruption of Mt. Pinatubo in 1991. Suites of balloon-borne instruments on a series of launches from Réunion Island intercepted the HT-HH plume within two weeks of the eruptions, yielding observations of the aerosol number and size distribution, and sulfur dioxide (SO_2) and water vapor (H_2O) concentrations. The measurements reveal an unexpected abundance of large particles in the plume, constrain the total sulfur injected to approximately 0.20 Tg, provide information on the altitude of the injection, and indicate that the formation of sulfuric acid aerosol was complete within three weeks. Large H_2O enhancements contributed as much as ~30% to ambient aerosol surface area and likely accelerated SO_2 oxidation and aerosol formation rates in the plume to ~ 3 times faster than under normal stratospheric conditions.

Significance Statement

Large volcanic eruptions can play an important role in Earth's radiative balance through stratospheric injections of sulfur dioxide that form sulfate aerosol. Here, we show that in situ observations are critical to constrain the injection mass of stratospheric sulfur and the stratospheric lifetime of sulfur dioxide. Such information is needed to better represent aerosol microphysics and improve predictions of the impacts of natural (or potentially anthropogenic) sulfur dioxide injections. Measurements in the fresh volcanic Hunga Tonga-Hunga Haʹapai plume in January 2022 revealed that stratospheric aerosol formation ended ~3 times faster than is typical in the presence of a large amount of water vapor, resulting in a high signal in aerosol extinction from an abundance of large particles.

Main

73
74   Volcanic plumes that reach the stratosphere can influence Earth's radiative balance and
75   are a significant driver of climate variability (1). Under background conditions, sustaining the
76   stratospheric aerosol burden requires the addition of ~ 0.1 Tg sulfur (S) yr^{-1} from the oxidation of
77   carbonyl sulfide and sulfur dioxide (SO_2) (2), while stratospheric transport (3) and a variety of
78   localized aerosol processes (4) contribute to heterogeneity in aerosol number and size.
79   Simulating an eruption's impact on stratospheric aerosol requires either knowledge or
80   assumptions of its injection height and mass (5), plume composition, location, and atmospheric
81   state. In situ measurements within one to three weeks of an eruption can provide critical
82   information for improving these assumptions.
83   The energetic eruption of the underwater Hunga Tonga-Hunga Haʹapai (HT-HH) volcano
84   (20.54 °S, 175.38 °W) on Jan. 15 (04:00 UTC) (6), together with a smaller eruption on Jan. 13
85   (15:20 UTC), injected an estimated 150 Tg water vapor (H_2O) (7) and 0.41 ± 0.01 Tg SO_2 into
86   the stratosphere (7, 8). The combination of its explosivity and the extraordinary amount of H_2O
87   injected into the stratosphere make the Jan. 15 eruption unique in the satellite era. Estimated
88   injection heights for these two eruptions ranged from 20 km on Jan. 13 to > 30 km on Jan. 15,
89   and the SO_2 plumes quickly overlapped, making them difficult to distinguish (8). Radiosonde
90   measurements reveal enhanced H_2O between 19 km and the maximum altitude of balloon
91   soundings, near 30 km (9). The HT-HH aerosol layer generated the highest signal in
92   stratospheric aerosol optical extinction since the eruption of Mt. Pinatubo in 1991 (10). Given the
93   relatively small injections of SO_2 (7, 8) by the HT-HH eruptions, the large signal in aerosol
94   extinction sparked questions regarding the initial S injection (11), the role of H_2O in rapid
95   aerosol formation in this plume and its timeline (12, 13).
96   In situ observations of particle number concentration and size distribution complement
97   space-based aerosol retrievals. For the first three months after the HT-HH eruption, the Ozone
98   Mapping and Profiler Suite-Limb Profile (OMPS-LP) sensor onboard the Suomi National Polar-
99   orbiting Partnership (S-NPP) satellite supplied a continuous global record of the main volcanic
100 plume's altitude between 16 – 30 km, its horizontal extent and its impact on stratospheric aerosol
101 optical depth (sAOD) (10). The Tonga volcano Rapid Response Experiment (TR^{2}Ex) provided
102 high-resolution vertical profiles with relatively low uncertainty of SO_2 (14) and H_2O (15, 16) to
103 ~ 30 km altitude and information on the aerosol size distribution in the main plume, which
104 cannot be reliably inferred from either satellite or ground-based measurements. Here, we
105 leverage a combination of these in situ measurements and OMPS-LP retrievals (17) to address
106 questions regarding the HT-HH eruption's impact on the lifetime of SO_2 and the magnitude and
107 altitude of the initial sulfur injection.
108
109
Results
110
111 1.Rapid Response Insights
112   TR^{2}Ex was a unique deployment of a suite of balloon-borne instrumentation that
113 repeatedly analyzed the composition of the volcanic plume 7 – 10 days after the second, larger
114 HT-HH eruption. Sampling the fresh HT-HH plume yielded in situ observations of aerosol size
115 distribution, SO_2, and H_2O at several pivotal times during its evolution (see Methods, Section 1
116 for details; Table S1). In situ measurements from this campaign allow us to quantify the S
117 gas/particle phase partitioning within the plume, study the vertical distribution of the S injection,

118 and explore the role of stratospheric H_2O enhancements in increasing ambient aerosol size and
119 extinction.
120   Portable Optical Particle Spectrometer (POPS) (18) measurements during TR^2Ex show
121 the impact of the HT-HH eruption on aerosol dry mass and extinction (enhancements ranged
122 from two to three orders of magnitude), driven by high concentrations of large accumulation
123 mode aerosols in the volcanic plume (Fig. 1; see Methods, Section 2 for details). By the time the
124 plume reached La Réunion seven days after the second eruption, wind shear had stretched the
125 initial injection into a thin slanted layer of varying thickness as it moved west (19). Positive
126 altitude gradients in easterly windspeeds resulted in progressively shorter transit times with
127 increasing altitude. TR^2Ex instruments were unable to measure two isolated optically thin
128 volcanic aerosol layer segments detected above 30 km by space-based and ground-based remote
129 sensing instruments (10, 19)— as these were above the operation ceiling of balloon sondes. Parts
130 of the aerosol layer between 25 km and 28 km (Fig. 1c-d) corresponded to a region with a
131 substantial H_2O enhancement (Fig. S1). Particle number concentration of both large and small
132 particles (up to 1.5 μm) was as much as three orders of magnitude higher than in unperturbed air
133 masses. The mode of the size distribution occurred at ~ 560 nm diameter, and the aerosol
134 effective radius exceeded 0.3 μm (Fig. S2). With H_2O enhancements of ~340 ppmv in this part
135 of the plume, H_2O contributed ~ 15% to the aerosol diameter at ~ 560 nm and ~ 30% to the total
136 aerosol surface area (Fig. S3; see Methods, Section 2). Differences in aerosol surface area impact
137 both extinction and stratospheric chemistry (20), highlighting the importance of calculating
138 ambient aerosol size related to the HT-HH eruption. The air was much drier (< 17 ppmv H_2O) in
139 the part of the plume below 25 km, which contained an elevated number concentration of
140 particles < 700 nm in diameter. The highest number concentration below 25 km occurred at the
141 smallest particle size (Fig. 1e-f), and the aerosol effective radius was not noticeably different
142 from baseline values (~ 0.2 μm; Fig. S2). Larger particles appeared more often in the wetter,
143 higher altitude parts of the aerosol layer, presumably due to shorter SO_2 lifetimes and particle
144 coagulation within the plume (12).
145   On three occasions, simultaneous in situ measurements of SO_2 and aerosol in the volcanic
146 plume reveal varying rates of aerosol formation. Particles in the plume are presumed to be
147 composed of sulfuric acid (H_2SO_4) formed from SO_2 oxidation and are designated estimated
148 H_2SO_4 ($_eH_2SO_4$) (see Methods, Section 2 for details). Comparisons are shown between the mass
149 mixing ratios of S in $_eH_2SO_4$ and SO_2 (Fig. 2a-c). The altitudes of SO_2 enhancements and aerosol
150 accumulations correspond well, and the mass mixing ratios of S in $_eH_2SO_4$ exceeded those of S
151 in SO_2 on two of three flights. Outside of the fresh HT-HH plume, the SO_2 partial pressure was
152 below the detection limit of the SO_2 sonde. If SO_2 gas phase oxidation had proceeded at its
153 typical rate (i.e., an e-folding stratospheric lifetime, τ_{strat} = ~ 30 days) (21) after the two HT-HH
154 eruptions, we would expect a $\leq$30% estimated H_2SO_4 ($_eH_2SO_4$) aerosol to $\geq$70% SO_2 split (by S
155 mass) on Jan. 25,~ 10.5 days after the second, larger eruption. In the wetter, higher altitude
156 region of the plume, measured on Jan. 22, $_eH_2SO_4$ aerosol accounted for 90% of the total S in the
157 plume (Fig. 2d), implying a τ_{strat} = ~ 3 days. In a drier part of the aerosol layer encountered on
158 Jan. 24 at 22 km, $_eH_2SO_4$ aerosol constituted 68% of the total S (τ_{strat} = ~ 8 days), and on Jan. 25
159 at 20 km, only 35% of the total S (τ_{strat} = ~ 24 days). We infer that SO_2 oxidation in the fresh
160 plume proceeded at different rates as a function of H_2O, namely more quickly where H_2O mixing
161 ratios were higher due to an increased concentration of hydroxyl radicals (22, 23). These
162 measurements also provide information on the vertical distribution of the S injection (i.e., the
163 sum of the S in both SO_2 and in $_eH_2SO_4$ aerosol; Fig. 2d). The total S column mass of the higher

164 altitude part of the plume measured on Jan. 22 was nearly four times that of the lower altitude
165 part of the plume measured on Jan. 24 and 25, suggesting that the majority of SO_2 was injected
166 above 25 km (Fig. 2d).
167
168 2. Aerosol burden and stratospheric lifetime (τ_{strat}) of SO_2
169   Quantifying the S burden in the tropical HT-HH aerosol layer helps constrain the
170 stratospheric S injection and the τ_{strat} of SO_2, which are critical for model validation and have
171 widespread implications for stratospheric chemistry. The calculation relies on the relationship
172 between the aerosol S column and sAOD calculated using POPS size distributions on launches
173 from La Réunion and on OMPS-LP retrievals of sAOD (see Methods, Section 3). As the plume
174 moved westwards, TR^{2}Ex launches sampled its core on Jan. 22 – 23 and trailing edge on Jan. 24
175 – 25 (Fig. 3). The S in the $_eH_2SO_4$ aerosol layer grew from 0.03 Tg S on Jan. 18 to 0.15 Tg S on
176 Jan. 26 and reached a maximum of 0.18 Tg S on Feb. 3 (Fig. 4a). We estimate that on Jan. 23, ~
177 3/4 of the S mass was located in the higher altitude part of the aerosol layer, west of La Réunion
178 (Fig. 4a; Methods, Section 3). Leading up to the eruptions (i.e., on Jan. 10), the S burden in
179 background $_eH_2SO_4$ aerosol was < 0.001 Tg S. This result suggests that rapid aerosol conversion
180 took place: within ~ 19 days, all the SO_2 released from the eruptions, corresponding to as much
181 as 0.18 Tg S (8), was oxidized and converted to particles ($\geq$ 140 nm). By tracking the
182 accumulation of S in $_eH_2SO_4$ aerosol, we calculate the average τ_{strat} as ~ 10 –13 days in the plume
183 (see Methods, Section 4; Fig. 4b). We note, however, that if a sizeable fraction (e.g., 0.09 Tg) of
184 the aerosol mass were not composed of H_2SO_4, this would yield a longer estimated τ_{strat} (~ 14 –
185 17 days) given the same SO_2 injection. A short τ_{strat}, compared with the typical value of one
186 month under climatological stratospheric conditions, helps explain the rapid production of large
187 particles in the HT-HH plume and signals greater availability of the hydroxyl radical to react
188 with methane and trace gases in the stratosphere (12, 22, 23).
189
190 **Discussion**
191   A rapid response to large or unusual volcanic eruptions with in situ observations can
192 provide insight into the resulting aerosol microphysics, complement space-based aerosol
193 retrievals (7, 8, 10), and be essential to evaluate models. Together with satellite retrievals of
194 sAOD, POPS vertical profiles of particle size distributions enable the calculation of the aerosol
195 layer's S mass and the mean τ_{strat} of SO_2. We determined that $_eH_2SO_4$ formation was complete
196 within three weeks, which is consistent with a maximum effective radius (> 0.4 μm) observed in
197 early February (Fig. S2). In situ measurements of SO_2 and $_eH_2SO_4$ and calculations of the aerosol
198 layer's $_eH_2SO_4$ mass provide evidence that the bulk of the total S was injected above 25 km,
199 which cannot be easily deduced from satellite retrievals of SO_2 and aerosol extinction (8, 10).
200 These observations also indicate that SO_2 oxidation and aerosol conversion occurred at varying
201 rates within the plume, corresponding to localized H_2O enhancements. Radiosonde
202 measurements confirm that H_2O mixing ratios within the plume spanned more than an order of
203 magnitude (< 100 ppmv to > 1000 ppmv) (9). Climatological lower stratospheric mixing ratios in
204 the tropics do not typically exceed 4-5 ppmv (24). SO_2 oxidation and aerosol conversion took
205 place ~ 3 times faster, on average, than under climatological stratospheric conditions. SO_2
206 oxidation accelerates substantially in the presence of H_2O enhancements (12, 22, 23, 25). A short
207 τ_{strat} of SO_2 reflects the heightened oxidative capacity of the atmosphere, with important
208 implications on stratospheric chemistry and composition.

209   Our measurements clarify the contributions to aerosol extinction from H_2O after the HT-
210   HH eruptions, which has spurred discussion in the scientific community (10–13). We caution
211   against conflating a response in the aerosol extinction with a similar change in aerosol mass for
212   two reasons: H_2O contributed ~30% to aerosol extinction in the fresh HT-HH plume. Light
213   scattering efficiency is closely related to aerosol size, with a maximum efficiency (per unit
214   volume) at 500 nm diameter (20). Due to the 560 nm diameter mode of the measured aerosol size
215   distribution mode, the HT-HH aerosol layer resulted in a high sAOD relative to its injected mass.
216   Radiosonde measurements show similarly elevated H_2O throughout the plume between Jan. 20
217   and Feb. 1 (one quarter of the observations between 26 – 28 km altitude from all vertical profiles
218   during this period had $7 \leq H2O \leq 130$ ppmv) (26), signifying widespread implications for
219    $_eH_2SO_4$ particle size and the S mass in the higher altitude part of the aerosol layer. Particle size
220   distributions show that differences in the peak and shape of the size distribution result in
221   substantial differences in aerosol extinction (e.g., Fig. 1). Questions remain about how H_2O and
222   other compounds reaching the stratosphere during an eruption might influence aerosol
223   microphysics, including the propensity for new particle formation, condensation onto existing
224   particles, and particle coagulation.
225   TR[2]Ex serves as a roadmap for future rapid response campaigns to volcanic eruptions and
226   other stratospheric perturbations. Campaigns such as TR[2]EX further the understanding of aerosol
227   processes in the stratosphere and inform models predicting climate impacts under a variety of
228   past and potential future conditions. Stratospheric aerosol injection (SAI), one proposed method
229   of climate intervention, would entail a large anthropogenic addition of stratospheric aerosol. The
230   suite of instruments described here is capable of identifying potential SAI implementations,
231   providing insight into the aerosol composition (i.e., sulfate or other) and hygroscopic effect, and
232   could enable quantifying the mass (and altitude) of SAI.
233
234   **Methods**
235   1. Rapid Response Overview
236   POPS in situ observations (18) of aerosol size distributions were made as part of the
237   National Oceanic and Atmospheric Administration (NOAA) Earth Radiation Budget program's
238   Baseline Balloon Stratospheric Aerosol Profiles (B[2]SAP) project (27). The B[2]SAP project
239   combines intensive periods of operation (IOP) with routine baseline measurements in the
240   northern and southern hemispheres. For the Tonga volcano Rapid Response Experiment (TR[2]Ex)
241   between Jan. 21 and Jan. 26, B[2]SAP IOP activities were coordinated with additional sonde and
242   lidar measurements at the Maïdo Observatory (28) on La Réunion (21 °S, 55 °E). TR[2]Ex balloon
243   payloads consisted of either: (A) a POPS, a sulfur dioxide (SO_2) sonde, an Electrochemical
244   Concentration Cell (ECC) ozonesonde and a radiosonde, or (B), an ECC ozonesonde, a Compact
245   Optical Back-scatter Aerosol Detector (COBALD) instrument and a radiosonde (Table S1;
246   COBALD, ozonesonde, and lidar measurements are discussed elsewhere (19). The ground-based
247   lidars and the COBALD provided information on aerosol extinction (18) and backscattering,
248   respectively. Unfortunately, quantitative information on the aerosol depolarization in the plume
249   during TR[2]Ex does not exist because the lidar at the Maïdo observatory was not calibrated for
250   depolarization. Subsequent POPS and NOAA Frost point Hygrometer (FPH) launches in
251   February, March, and June 2022 at the Maïdo Observatory were part of what are now routine
252   B[2]SAP soundings (Table S1) (27).
253   SO_2 sonde (14) measurements have lower uncertainty and considerably better vertical
254   resolution than satellite SO_2 retrievals (8), particularly after an energetic volcanic eruption. A

255   modified ECC ozonesonde, the SO_2 sonde removes ozone from the sample prior to detection
256   using a filter, allowing stratospheric as well as tropospheric SO_2 to be quantified using pre-flight
257   calibrations (14). The SO_2 sonde has a ~ 25 sec response time, similar to that of an ozonesonde.
258   SO_2 data (Fig. 2) reflect a correction for this time (and altitude) lag (29, 30). CFH (31) and FPH
259   (16) instruments measuring H_2O were used to calculate ambient particle size, and Ozone
260   Mapping and Profiler Suite-Limb Profile (OMPS-LP) retrievals (17) were used to calculate the
261   volcanic plume's aerosol burden, as described below.
262
263   2. The POPS measurements and inherent assumptions
264   Particle sizing inherently requires assumptions about particle morphology and refractive
265   index related to aerosol composition (18). Here, we assume that particles are spherical and
266   composed of sulfuric acid (H_2SO_4) and water, with a corresponding refractive index of 1.45 at
267   405 nm (the wavelength of the POPS laser), leading to a reported particle number and size
268   distribution between 140 nm – 2.5 µm in diameter. Telemetered data are quality assured based
269   on available engineering parameters, including the instrument temperature, measured with a
270   thermistor located on the POPS laminar flow element, and the instrument flow (27). Particles are
271   expected to be at (or close to) equilibrium with the instrument temperature at the time of
272   detection, given a particle transit time of 60 – 90 ms. We note that POPS particle transit times
273   exceeded modeled timescales required for aerosol growth or evaporation within the plume, in
274   line with similar calculations from Kovilakam and Deshler (32) and Jonsson et al. (33).
275   The S in the $_eH_2SO_4$ aerosol column mass and mass mixing ratios are calculated from the
276   measured aerosol size distribution and particle density. The aerosol weight (wt.%) $_eH_2SO_4$ can be
277   determined using the partial pressure of H_2O at a range of temperatures (34–37). We apply the
278   formulation of Tabazedah et al. (37), which is suitable for low temperatures observed in the
279   lower stratosphere (when $_eH_2SO_4 \leq 80$ wt. %) and is based on Steele and Hamill (35), and the
280   expression of Gmitro and Vermeulen when $_eH_2SO_4 > 80$ wt. % (34). In the stratosphere,
281   particles have a calculated $\geq 80\%$ wt% $_eH_2SO_4$ at the time of detection due to instrument
282   temperatures (268 – 278 K) that are considerably higher than ambient stratospheric air ($\Delta T = 50$
283   – 75 K). Particle density at the time of detection is both wt.% and temperature dependent (38–
284   40). We use two parameterizations valid for temperatures between 233 – 298 K given different
285   wt. % (39, 40).
286   Ambient particle diameter is calculated according to Steele and Hamill (35) from the
287   measured (dehydrated) particle diameter, the particle wt. % and density both at the time of
288   detection and in ambient air, assuming that the particle was at equilibrium in both cases, and that
289   only water (not H_2SO_4) was lost from the particle during sampling (Fig. S2a). Measured aerosol
290   size distributions were averaged into 100 m altitude bins, to improve counting statistics and
291   facilitate the requisite merges with frost point hygrometer data from other launches. Possible
292   errors in measured particle sizing are driven primarily by Mie resonances (18). Uncertainty in
293   H_2O (<=6%), air temperature (< 1%), and uncertainties in the parameterizations of the wt. % and
294   density contribute additionally to possible errors in calculated ambient sizing (Fig. S2), and the
295   calculated S in $_eH_2SO_4$ mass mixing ratios and column mass (Fig. 2).
296   As in situ size distribution measurements provide no information on aerosol composition,
297   we cannot rule out the possibility that aerosol could have consisted of ash or some other material,
298   such as sea salt, coated (or internally mixed) with H_2SO_4. Contributions from HNO_3 aerosol or
299   mixtures containing HNO_3 and H_2SO_4 were considered but dismissed based on equilibrium
300   calculations (33, 41, 42). Although volcanic lightning on Jan. 15 (43) may have injected NO

301 directly into the stratosphere, HNO_3 hardly condenses at temperatures ≥ 220 K observed in the
302 plume, despite large enhancements in stratospheric H_2O.
303   The assumptions made here regarding particle composition and morphology are
304 supported by space-based Cloud-Aerosol Lidar with Orthogonal Polarization (CALIOP)
305 retrievals and geostationary satellite RGB-Ash composite imagery within the first few days of
306 the HT-HH eruption on Jan. 15 (11). CALIOP retrievals showed particles with low
307 depolarization, indicating spherical H_2SO_4 particles moving westward towards La Réunion on
308 Jan. 20. The geostationary satellite RGB-Ash composite images depicted a concomitant light
309 green SO_2 plume (with little to no ash) during this period.
310
311 3. Calculating the aerosol column and plume S burden
312   Vertical profiles of aerosol extinction at 997 nm, corresponding to the native wavelength
313 of the OMPS-LP sensor, are calculated using publicly available Mie codes (44, 45) and the
314 calculated particle size distribution in ambient air. POPS stratospheric ambient aerosol optical
315 depth (sAOD) is the sum of calculated ambient aerosol extinction above the tropopause.
316 Similarly, the POPS stratospheric S column in $_eH_2SO_4$ aerosol (g S m^{-2}) at a single geographic
317 location is quantified as the sum of the S in $_eH_2SO_4$ aerosol (µg S m^{-2} air) in each 100 m altitude
318 bin above the tropopause. A baseline value of the S column in $_eH_2SO_4$ aerosol, calculated from a
319 vertical profile outside the plume on Jan. 23 (14 UTC), was subtracted from each measurement
320 that encountered the plume to determine the S in the aerosol layer (g S m^{-2}). Because SO_2
321 measurements were below the SO_2 sonde's limit of detection outside the plume, no similar
322 subtraction of the S column in SO_2 under baseline conditions was made following integration for
323 comparisons in Figure 2d.
324   A linear regression between the POPS calculated ambient sAOD and S in $_eH_2SO_4$ column
325 mass enables global retrievals of OMPS-LP sAOD to be used to infer the S column mass across
326 the entire aerosol layer and track the S aerosol burden as the plume evolves. Estimates of the
327 $_eH_2SO_4$ aerosol layer mass, based on relationships between the POPS measured (dehydrated)
328 sAOD and POPS stratospheric S column ($\pm$ uncertainty) and the calculated ambient sAOD and
329 POPS stratospheric S column ($\pm$ uncertainty) over La Réunion between Jan. 22 and Jun. 9 are
330 shown in Figure S4a. The reported uncertainty in OMPS-LP sAOD signal in the stratosphere
331 (10% at $\lambda = 997\ nm$) (17) is negligeable compared to the differences in the slope and intercept
332 POPS sAOD vs. mass relationships (Fig. S4a). We note that recent debate with respect to
333 potential OMPS-LP retrieval biases (46) is beyond the scope of this work but would lead to a
334 lower $_eH_2SO_4$ aerosol layer mass. The maximum value of daily sAOD from the OMPS-LP sensor
335 on Jan. 10 (50 °S – 50 °N) was used as the sAOD threshold to identify the geographic extent of
336 the tropical HT-HH aerosol layer (Fig. S4b); its median (0.0025) was used as a background
337 sAOD value in the tropics. The linear relationships from Fig. S4a were applied to each daily
338 sAOD value in the aerosol layer to infer the S column (g S m^{-2}) in each (2° latitude x 24°
339 longitude) grid cell. The resulting S column using the relationship between the ambient sAOD
340 and S in $_eH_2SO_4$ column mass is shown in Figure 3. For reference, the H_2O plume extent,
341 calculated from MLS retrieval levels between 10 and 46 hPa using MLS H_2O anomalies between
342 Jan. 21 – Jan. 23 (defined as the median $\pm$ 3 x the mean absolute deviation) is also shown in
343 Figure 3c, compared to the aerosol layer.
344   The S column was then multiplied by the area of the corresponding geographic grid cell
345 (m^2) and summed to determine the total stratospheric S burden (Tg S) over that area. By
346 applying the relationships from Fig. S4a to the background sAOD value, multiplied by the

347   aerosol layer's geographic area, we similarly calculated the corresponding S burden under
348   background conditions in each case. The S burden under background conditions was then
349   subtracted from the total stratospheric aerosol S burden to yield the volcanic aerosol layer's S
350   burden $\pm$ uncertainty (Tg S) shown in Figure 4. The uncertainty in the S burden (the shaded
351   black region) reflects the range of the estimates shown in Figure S4a. The S mass in the upper
352   part of the plume was approximated as the sum of the S burden (in $_eH_2SO_4$ aerosol) west of La
353   Réunion (55° E), when the higher altitude part of the aerosol layer was last observed on Jan. 23
354   00 UTC (Fig. 1d)(19). La Réunion is located near the latitudinal edge (48° E) of two adjacent
355   OMPS-LP grid-cells. Thus, this estimate represents the arithmetic mean
356   ($\pm$ the standard deviation) of the S burden in the adjacent OMPS-LP grid cells centered at 36°
357   E and 60° E (Fig. 4).
358
359   4. Estimating the SO_2 lifetime
360   By monitoring the aerosol loading following an eruption, we can estimate the initial
361   injection of S and subsequently deduce the stratospheric lifetime (τ_{strat}) of SO_2. We assume that
362   all the SO_2 is converted to H_2SO_4:
363

364    $$1. \frac{d[H_2SO_4]}{dt} = -\frac{d[SO_2]}{dt}, \text{and } [SO_2] = [SO_{2\,t=0}] - ([H_2SO_4] - [H_2SO_{4_{t=0}}])$$

365
366   Making these substitutions into the first order rate law $\frac{d[SO_2]}{[SO_2]} = -kdt$ and integrating

367   demonstrates that the amount of H_2SO_4 produced depends on the initial injection of SO_2 and on
368   the background H_2SO_4 burden (together with any initial injection of aerosol) and enables us to
369   calculate τ_{strat} of SO_2 through linear regression against t (elapsed days since 4:00 UTC on Jan.
370   15), where k is the slope of the line and $\tau_{strat\,=}1/k$:
371

372    $$2. \ln \frac{[SO_{2\,t=0}]}{[SO_{2\,t=0}] - ([H_2SO_4] - [H_2SO_{4_{t=0}}])} = kt$$

373
374   The initial injection of S, $SO_{2\,t=0}$, is based on satellite retrievals of SO_2, which are slightly greater
375   than the maximum accrual of S in $_eH_2SO_4$ aerosol after the eruption (0.190 Tg; Fig. 4a). τ_{strat} was
376   calculated using a range of values for the initial SO_2 injection (0.195 – 0.215 Tg S in SO_2). Prior
377   to the eruption (e.g, on Jan. 10), the initial S burden in the aerosol layer is close to zero (0.0005
378   Tg S in $_eH_2SO_4$), which is used as the value for $H_2SO_{4\,t=0}$. If as much as 0.09 Tg of aerosol mass
379   were not composed of H_2SO_4 (0.03 Tg S is in 0.09 Tg $_eH_2SO_4$) this would result in an estimated
380   τ_{strat} of 15-17 days. Equation 2 ignores a potential time lag required for either particle formation
381   or aerosol growth through condensation to particle diameter ≥ 0.14 µm from H_2SO_4 gas,
382   considered negligible in this case.
383

384   **Data Availability**
385   The processed POPS aerosol size distribution data from all launches used in this study
386   may be found under the supporting data tab for this manuscript at
387   https://csl.noaa.gov/projects/b2sap/data.html, where processed SO_2 and H_2O data from TR[2]Ex,
388   and processed daily files of OMPS-LP sAOD and MLS H_2O plume areas and anomalies from 21
389   hPa are also available. Raw OMPS-LP and MLS H2O data may be found at

Open Access

Competing interests

Materials and Correspondence

Corresponding author, Elizabeth Asher (Elizabeth.asher@noaa.gov) should be contacted
with any questions or requests for material.

References

1. S. Solomon, *et al.*, The Persistently Variable "Background" Stratospheric Aerosol Layer
   and Global Climate Change. *Science* **333**, 866–870 (2011).

2. A. Feinberg, *et al.*, Improved tropospheric and stratospheric sulfur cycle in the aerosol–
   chemistry–climate model SOCOL-AERv2. *Geosci. Model Dev.* **12**, 3863–3887 (2019).

3. M. H. Hitchman, M. McKay, C. R. Trepte, A climatology of stratospheric aerosol. *J.
   Geophys. Res.* **99**, 20689 (1994).

4. S. Kremser, *et al.*, Stratospheric aerosol-Observations, processes, and impact on climate:
   Stratospheric Aerosol. *Rev. Geophys.* **54**, 278–335 (2016).

5. L. O. Muser, *et al.*, Particle aging and aerosol–radiation interaction affect volcanic plume
   dispersion: evidence from the Raikoke 2019 eruption. *Atmospheric Chem. Phys.* **20**, 15015–
   15036 (2020).

431   6.   C. J. Wright, *et al.*, Surface-to-space atmospheric waves from Hunga Tonga–Hunga
432   Ha'apai eruption. *Nature* **609**, 741–746 (2022).

433   7.   L. Millán, *et al.*, The Hunga Tonga-Hunga Ha'apai Hydration of the Stratosphere. *Geophys.*
434   *Res. Lett.* **49** (2022).

435   8.   S. A. Carn, N. A. Krotkov, B. L. Fisher, C. Li, Out of the blue: Volcanic SO2 emissions
436   during the 2021–2022 eruptions of Hunga Tonga—Hunga Ha'apai (Tonga). *Front. Earth*
437   *Sci.* **10**, 976962 (2022).

438   9.   H. Vömel, S. Evan, M. Tully, Water vapor injection into the stratosphere by Hunga Tonga-
439   Hunga Ha'apai. *Science* **377**, 1444–1447 (2022).

440   10.   G. Taha, *et al.*, Tracking the 2022 Hunga Tonga-Hunga Ha'apai aerosol cloud in the upper
441   and middle stratosphere using space-based observations. *Geophys. Res. Lett.* (2022)
442   https:/doi.org/10.1029/2022GL100091 (October 2, 2022).

443   11.   B. Legras, *et al.*, The evolution and dynamics of the Hunga Tonga–Hunga Ha'apai sulfate
444   aerosol plume in the stratosphere. *Atmospheric Chem. Phys.* **22**, 14957–14970 (2022).

445   12.   Y. Zhu, *et al.*, Perturbations in stratospheric aerosol evolution due to the water-rich plume
446   of the 2022 Hunga-Tonga eruption. *Commun. Earth Environ.* **3**, 248 (2022).

447   13.   M. R. Schoeberl, *et al.*, Analysis and Impact of the Hunga Tonga-Hunga Ha'apai
448   Stratospheric Water Vapor Plume. *Geophys. Res. Lett.* **49** (2022).

449   14.   S. Yoon, *et al.*, Development and testing of a novel sulfur dioxide sonde. *Atmospheric*
450   *Meas. Tech.* **15**, 4373–4384 (2022).

451   15.   H. Vömel, T. Naebert, R. Dirksen, M. Sommer, An update on the uncertainties of water
452   vapor measurements using cryogenicfrost point hygrometers. *Atmospheric Meas. Tech.* **9**,
453   3755–3768 (2016).

454   16.   E. G. Hall, *et al.*, Advancements, measurement uncertainties, and recent comparisons of the
455   NOAAfrost point hygrometer. *Atmospheric Meas. Tech.* **9**, 4295–4310 (2016).

456   17.   G. Taha, *et al.*, OMPS LP Version 2.0 multi-wavelength aerosol extinction coefficient
457   retrieval algorithm. *Atmospheric Meas. Tech.* **14**, 1015–1036 (2021).

458   18.   R. S. Gao, *et al.*, A light-weight, high-sensitivity particle spectrometer for PM2.5 aerosol
459   measurements. *Aerosol Sci. Technol.* **50**, 88–99 (2016).

460   19.   A. Baron, *et al.*, Early Evolution of the Stratospheric Aerosol Plume Following the 2022
461   Hunga Tonga-Hunga Ha'apai Eruption: Lidar Observations From Reunion (21°S, 55°E).
462   *Geophys. Res. Lett.* **50**, e2022GL101751 (2023).

463 20. D. M. Murphy, *et al.*, Radiative and chemical implications of the size and composition of
464 aerosol particles in the existing or modified global stratosphere. *Atmospheric Chem. Phys.*
465 **21**, 8915–8932 (2021).

466 21. M. Höpfner, *et al.*, Sulfur dioxide (SO2) from MIPAS in the upper troposphere and lower
467 stratosphere 2002–2012. *Atmospheric Chem. Phys.* **15**, 7017–7037 (2015).

468 22. A. N. LeGrande, K. Tsigaridis, S. E. Bauer, Role of atmospheric chemistry in the climate
469 impacts of stratospheric volcanic injections. *Nat. Geosci.* **9**, 652–655 (2016).

470 23. J. H. Seinfeld, Pandis, Spyros N., *Atmospheric Chemistry and Physics: From Air Pollution*
471 *to Climate Change* (John Wiley & Sons, 2006).

472 24. D. F. Hurst, *et al.*, Recent divergences in stratospheric water vapor measurements by frost
473 pointhygrometers and the Aura Microwave Limb Sounder. *Atmospheric Meas. Tech.* **9**,
474 4447–4457 (2016).

475 25. Y. Zhu, *et al.*, Persisting volcanic ash particles impact stratospheric SO2 lifetime and
476 aerosol optical properties. *Nat. Commun.* **11**, 4526 (2020).

477 26. Vömel, Holger, Hunga Tonga-Hunga Ha'apai stratospheric water vapor from Vaisala RS41
478 radiosondes https:/doi.org/10.5065/P328-Z959 (September 25, 2022).

479 27. M. A. Todt, *et al.*, Baseline Balloon Stratospheric Aerosol Profiles (B ^{2} SAP)- Systematic
480 measurements of aerosol number density and size. *J. Geophys. Res. Atmospheres*,
481 e2022JD038041 (2023).

482 28. A. Baron, *et al.*, "Early evolution of the Hunga – Tonga Volcanic Plume from Lidar
483 Observations at Reunion Island (Indian Ocean, 21°S, 55°E)" (display, 2022)
484 https:/doi.org/10.5194/egusphere-egu22-13599 (February 5, 2023).

485 29. H. Vömel, *et al.*, A new method to correct the electrochemical concentration cell (ECC)
486 ozonesonde time response and its implications for "background current" and pump
487 efficiency. *Atmospheric Meas. Tech.* **13**, 5667–5680 (2020).

488 30. L.-J. Huang, M.-J. Chen, C.-H. Lai, H.-T. Hsu, C.-H. Lin, New Data Processing Equation to
489 Improve the Response Time of an Electrochemical Concentration Cell (ECC) Ozonesonde.
490 *Aerosol Air Qual. Res.* **15**, 935–944 (2015).

491 31. H. Vömel, D. E. David, K. Smith, Accuracy of tropospheric and stratospheric water vapor
492 measurements by the cryogenic frost point hygrometer: Instrumental details and
493 observations. *J. Geophys. Res.* **112**, D08305 (2007).

494 32. M. Kovilakam, T. Deshler, On the accuracy of stratospheric aerosol extinction derived from
495 in situ size distribution measurements and surface area density derived from remote SAGE
496 II and HALOE extinction measurements. *J. Geophys. Res. Atmospheres* **120**, 8426–8447
497 (2015).

12

498   33.   H. H. Jonsson, *et al.*, Performance of a Focused Cavity Aerosol Spectrometer for
499   Measurements in the Stratosphere of Particle Size in the 0.06–2.0-µm-Diameter Range. *J.*
500   *Atmospheric Ocean. Technol.* **12**, 115–129 (1995).

501   34.   J. I. Gmitro, T. Vermeulen, Vapor-liquid equilibria for aqueous sulfuric acid. *AIChE J.* **10**,
502   740–746 (1964).

503   35.   H. M. Steele, P. Hamill, Effects of temperature and humidity on the growth and optical
504   properties of sulphuric acid—water droplets in the stratosphere. *J. Aerosol Sci.* **12**, 517–528
505   (1981).

506   36.   S. L. Clegg, P. Brimblecombe, Application of a Multicomponent Thermodynamic Model to
507   Activities and Thermal Properties of 0−40 mol kg $^{-1}$ Aqueous Sulfuric Acid from <200 to
508   328 K. *J. Chem. Eng. Data* **41**, 1530–1530 (1996).

509   37.   A. Tabazadeh, O. B. Toon, S. L. Clegg, P. Hamill, A new parameterization of H_2SO_4/H_2
510   O aerosol composition: Atmospheric implications. *Geophys. Res. Lett.* **24**, 1931–1934
511   (1997).

512   38.   E. Washburn W., Ed., *International critical tables of numerical data, physics, chemistry*
513   *and technology* (McGraw-Hill, 1928).

514   39.   M. Kulmala, A. Laaksonen, L. Pirjola, Parameterizations for sulfuric acid/water nucleation
515   rates. *J. Geophys. Res. Atmospheres* **103**, 8301–8307 (1998).

516   40.   L. Oca, J. M. Campillo-Robles, M. M. Bou-Ali, Review and Analysis of Thermophysical
517   Properties of a Sulfuric Acid–Water Electrolyte. *J. Chem. Eng. Data* **63**, 3572–3583 (2018).

518   41.   M. D. Petters, S. M. Kreidenweis, A single parameter representation of hygroscopic growth
519   and cloud condensation nucleus activity. *Atmospheric Chem. Phys.* **7**, 1961–1971 (2007).

520   42.   Jack Alf Goff, S. Gratch, Low-pressure properties of water from -160 to 212 °F in
521   (Transactions of the American Society of Heating and Ventilating Engineers, 1946), pp.
522   95–122.

523   43.   D. A. Yuen, *et al.*, Under the surface: Pressure-induced planetary-scale waves, volcanic
524   lightning, and gaseous clouds caused by the submarine eruption of Hunga Tonga-Hunga
525   Ha'apai volcano. *Earthq. Res. Adv.* **2**, 100134 (2022).

526   44.   C. F. Bohren, D. R. Huffman, *Absorption and Scattering of Light by Small Particles*, 1st
527   Ed. (Wiley, 1998) https:/doi.org/10.1002/9783527618156 (September 23, 2022).

528   45.   B. J. Sumlin, W. R. Heinson, R. K. Chakrabarty, Retrieving the aerosol complex refractive
529   index using PyMieScatt: A Mie computational package with visualization capabilities. *J.*
530   *Quant. Spectrosc. Radiat. Transf.* **205**, 127–134 (2018).

531   46.   A. E. Bourassa, *et al.*, Tomographic Retrievals of Hunga Tonga-Hunga Ha'apai Volcanic
532   Aerosol. *Geophys. Res. Lett.* **50** (2023).

536 **Figures**
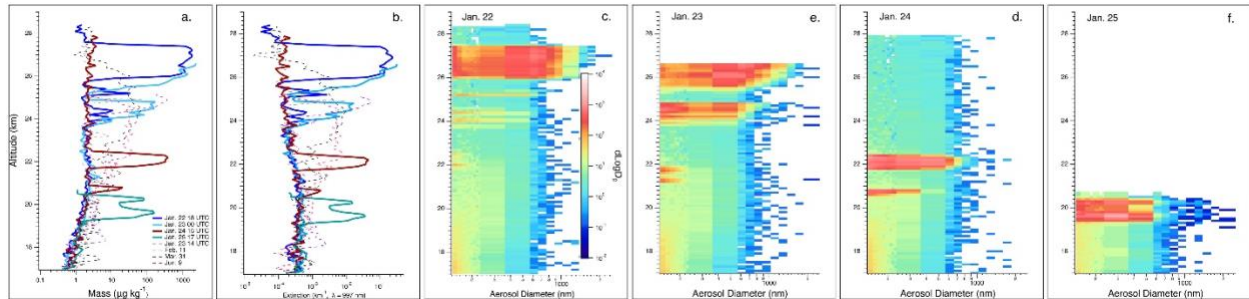
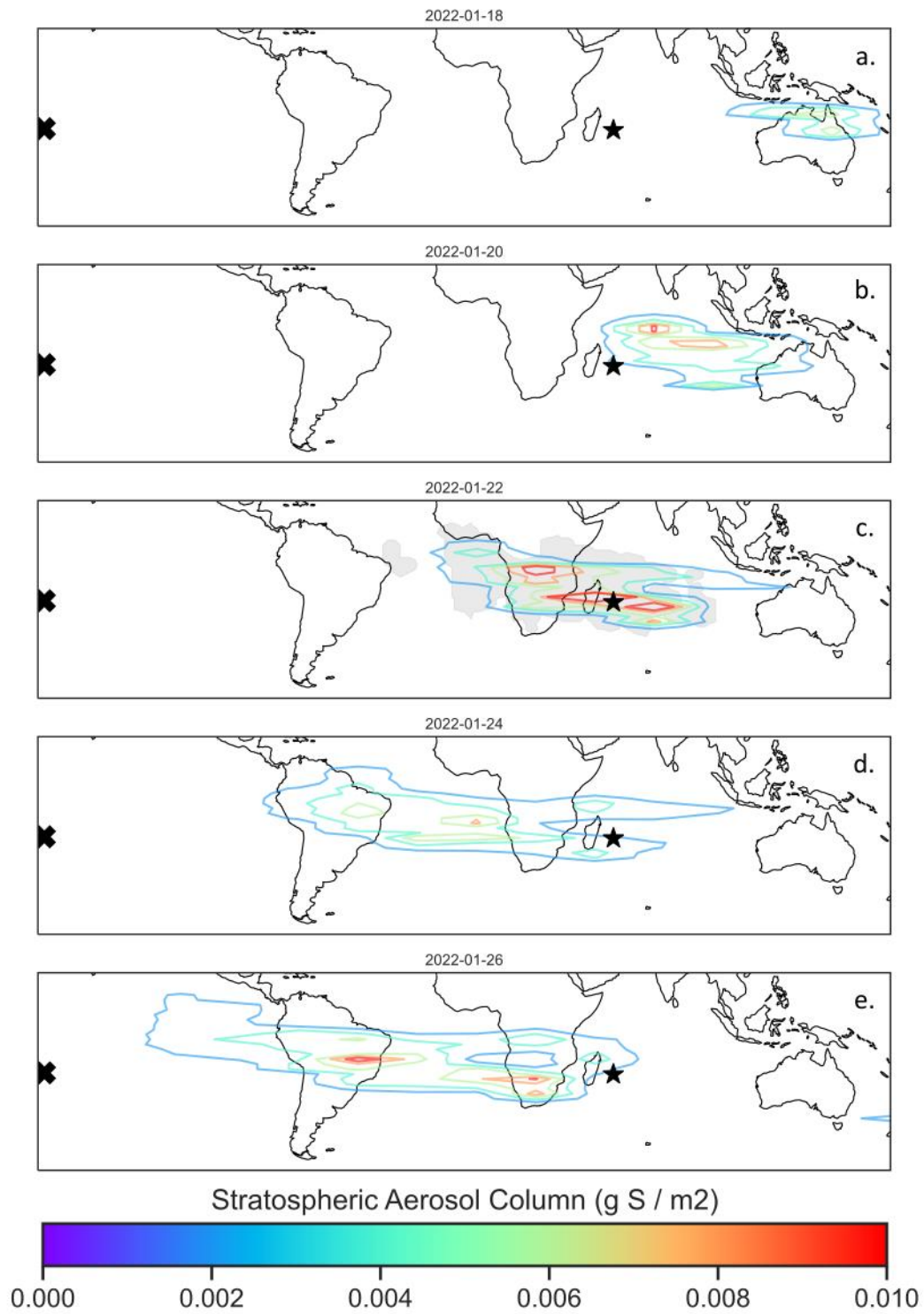540 **Figure 1.** Vertical profiles of calculated bulk aerosol properties between January and June 2022
541 (from POPS size distribution data), including mass mixing ratios (a) and ambient extinction
542 using Steele and Hamill (35)(b), both of which use the legend in panel (a), and vertical profiles
543 of the measured aerosol size distributions from TR^{2}Ex launches when the fresh HT-HH aerosol
544 plume was encountered (c, d, e, f). Aerosol size distributions (dN/dLogD$_p$) for the four TR^{2}Ex
545 soundings (c, d, e, f) use the color scale in panel (c).
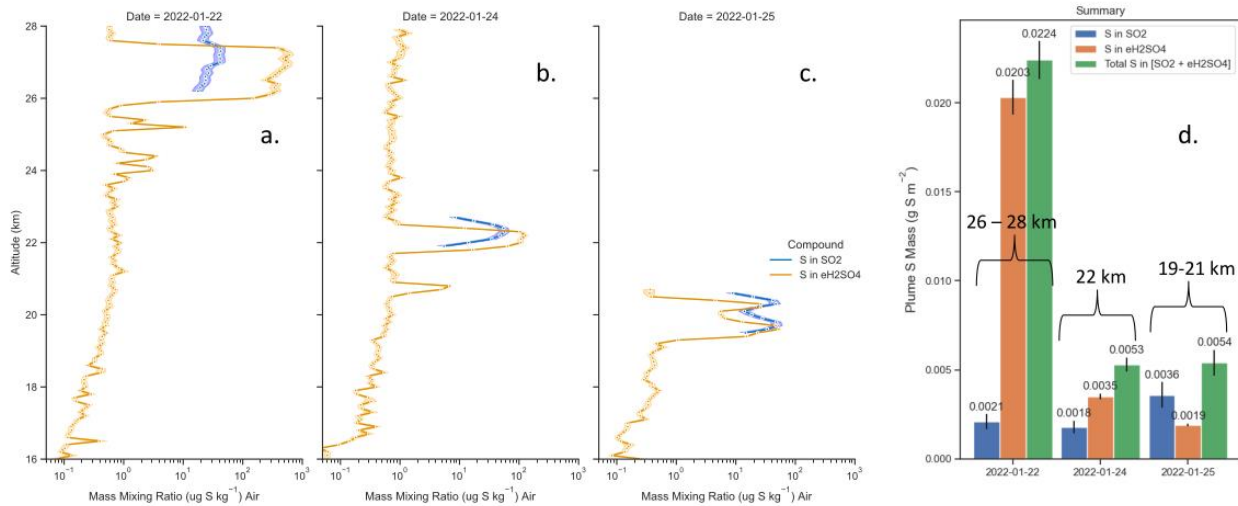
548 **Figure 2.** On three different dates, vertical profiles of S in SO$_2$ mass mixing ratios and calculated
549 S in $_e$H$_2$SO$_4$ mass mixing ratios based on aerosol size distributions, when both instruments
550 measured the volcanic plume with low uncertainties (a-c), and a summary of the S column mass
551 in SO$_2$, the S column mass in $_e$H$_2$SO$_4$, and the total S column mass ([S in SO2] + [S in $_e$H$_2$SO$_4$]
552 observed within the plume (d). Shaded areas and error bars show the uncertainty in SO$_2$ sonde
553 measurements (≤20%) and the uncertainty in calculated eH$_2$SO$_4$ mass mixing ratios and S mass
554 including possible error related to aerosol sizing and aerosol density.

14

2022-01-18

a.

2022-01-20

b.

2022-01-22

c.

2022-01-24

d.

2022-01-26

e.

Stratospheric Aerosol Column (g S / m2)

0.000   0.002   0.004   0.006   0.008   0.010

556
Figure 3. Contour plots of the $_eH_2SO_4$ aerosol column (g m^{-2}), calculated using the equation in
the Fig. S4a caption, for 5 days from Jan. 18 to Jan 26 (a-e). On Jan. 22, the gray shaded area

shows the maximum plume extent between Jan. 21 – Jan. 23 as determined from MLS H_2O
anomalies at 21 hPa. Locations of HT-HH and La Réunion are marked with a cross and star,
respectively.
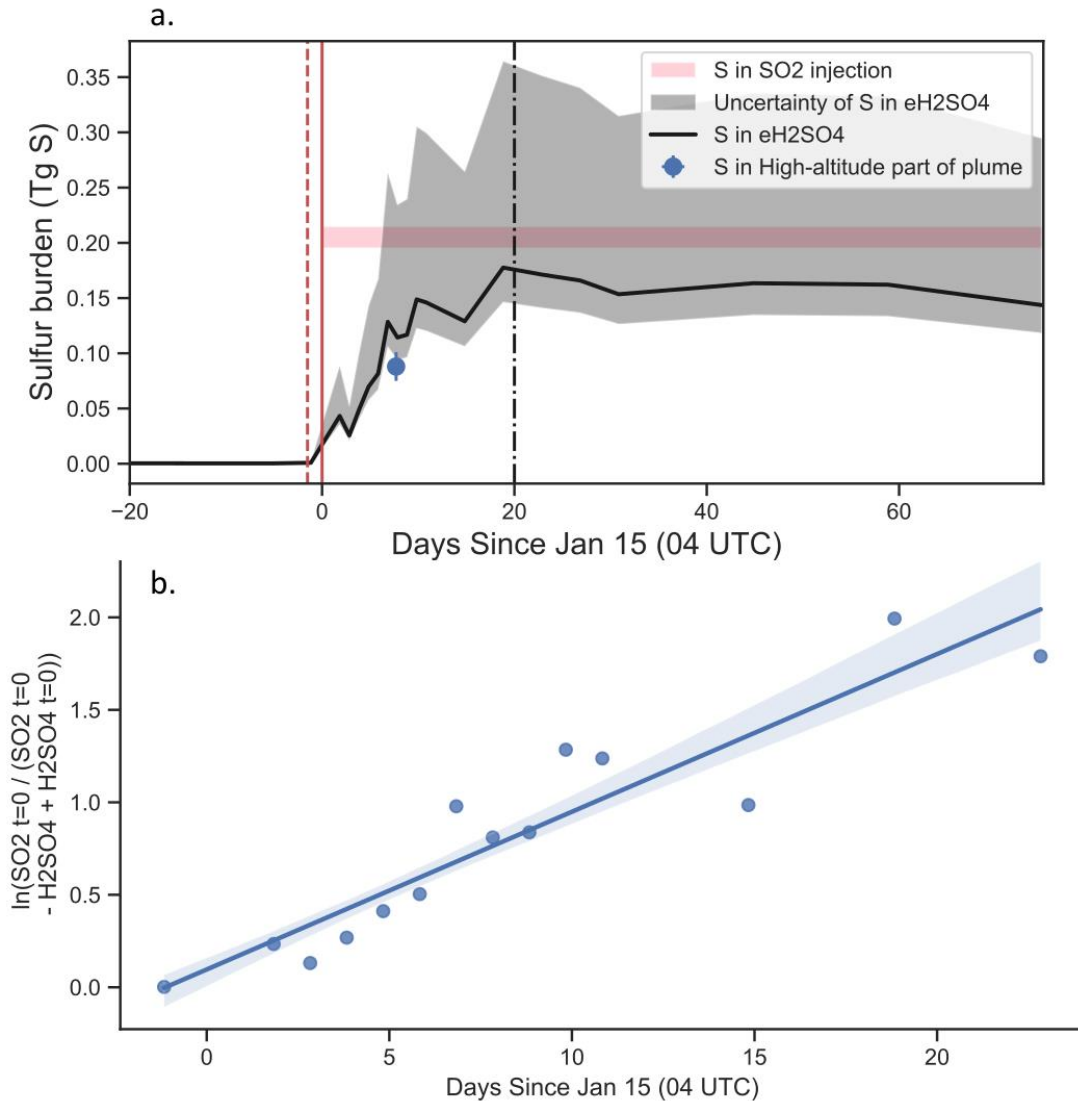
Figure 4. A time series of the calculated S burden in $_eH_2SO_4$ aerosol, calculated using a
combination of POPS measurements and OMPS-LP retrievals (a) and the estimation of the τ_{strat}
(b). The calculated S burden in $_eH_2SO_4$ aerosol (black line) represents the relationship between
calculated ambient sAOD and the mass, and agrees with estimates of the S injected as SO_2 from
satellites (7, 8) (pink shaded region). The uncertainty (black shaded region) represents the range
of assumptions considered in Figure S4a. The approximated S mass in the higher altitude part of
the plume, west of La Réunion on Jan. 23 00 UTC is also shown. OMPS-LP Dashed vertical
lines depict the period of $_eH_2SO_4$ aerosol accumulation. The S burden from this period is used to
calculate the stratospheric lifetime of SO_2, $\tau_{strat} = 1/k$, as shown in equation 3 (Methods

573   Section 3). Assuming an SO_2 injection of 0.205 Tg S in SO_2 (7, 8) $k = 0.10$ ($r^2 = 0.87$; $p <$
574   1.23E-6; 1 standard deviation of the slope is ± 0.011), suggesting a τ_{strat} for SO_2 of ~ 10 days (b).
575